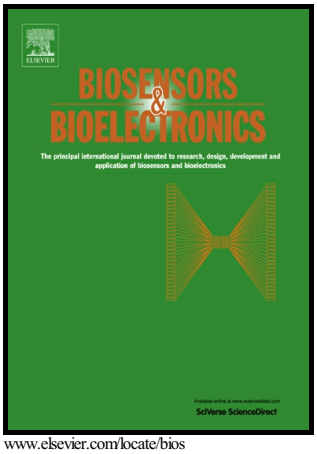

www.elsevier.com/locate/bios

The *MyoRobot*: a novel automated biomechatronics system to assess voltage/Ca^{2+} biosensors and active/passive biomechanics in muscle and biomaterials

M Haug, B Reischl, G Prölß, C Pollmann, T Buckert, C Keidel, S Schürmann, M Hock, S Rupitsch, M Heckel, T Pöschel, T Scheibel, C Haynl, L Kiriaev, SI Head, O Friedrich

PII: S0956-5663(17)30803-5
DOI: https://doi.org/10.1016/j.bios.2017.12.003
Reference: BIOS10148

To appear in: *Biosensors and Bioelectronic*

Received date: 7 August 2017
Revised date: 11 November 2017
Accepted date: 5 December 2017

Cite this article as: M Haug, B Reischl, G Prölß, C Pollmann, T Buckert, C Keidel, S Schürmann, M Hock, S Rupitsch, M Heckel, T Pöschel, T Scheibel, C Haynl, L Kiriaev, SI Head and O Friedrich, The *MyoRobot*: a novel automated biomechatronics system to assess voltage/Ca^{2+} biosensors and active/passive biomechanics in muscle and biomaterials, *Biosensors and Bioelectronic,* https://doi.org/10.1016/j.bios.2017.12.003

The *MyoRobot*: a novel automated biomechatronics system to assess voltage/Ca^{2+} biosensors and active/passive biomechanics in muscle and biomaterials

M Haug[1,#], B Reischl[1,#], G Prölß[1], C Pollmann[1], T Buckert[1,2], C Keidel[1,2], S Schürmann[1], M Hock[1], S Rupitsch[2], M Heckel[3], T Pöschel[3], T Scheibel[4,5], C Haynl[4], L Kiriaev[6,7], SI Head[6,7], O Friedrich[1,6,*]

[1] Institute of Medical Biotechnology, Friedrich-Alexander-University Erlangen-Nürnberg, Paul-Gordan-Str. 3, 91052 Erlangen, Germany
[2] Institute of Sensor Technology, Friedrich-Alexander-University Erlangen-Nürnberg
[3] Institute of Multi Scale Simulation of Particulate Systems, Friedrich-Alexander-University Erlangen-Nürnberg, Germany
[4] Institute of Biomaterials, University of Bayreuth, 95440 Bayreuth, Germany
[5] Bayerisches Polymerinstitut (BPI), 95440 Bayreuth, Germany
[6] School of Medical Sciences, Faculty of Medicine, University of New South Wales, Wallace Wurth Building, Sydney, NSW 2052 Australia
[7] Department of Physiology, School of Medicine, University of Western Sydney, Campbelltown Campus, Western Sydney, NSW, Australia

[#] these authors contributed equally

[*] Corresponding author, e-mail: oliver.friedrich@mbt.uni-erlangen.de

Running title: *MyoRobot* - an automated muscle/biopolymer biomechatronics system

Abstract

We engineered an automated biomechatronics system, *MyoRobot*, for robust objective and versatile assessment of muscle or polymer materials (bio-)mechanics. It covers multiple levels of muscle biosensor assessment, e.g. membrane voltage or contractile apparatus Ca^{2+} ion responses (force resolution 1 µN, 0-10 mN for the given sensor; [Ca^{2+}] range ~100 nM – 25 µM). It replaces previously tedious manual protocols to obtain exhaustive information on active/passive biomechanical properties across various morphological tissue levels. Deciphering mechanisms of muscle weakness requires sophisticated force protocols, dissecting contributions from altered Ca^{2+} homeostasis, electro-chemical, chemico-mechanical biosensors or visco-elastic components. From whole organ to single fibre levels, experimental demands and hardware requirements increase, limiting biomechanics research potential, as reflected by only few commercial biomechatronics systems that can address resolution, experimental versatility and mostly, automation of force recordings. Our *MyoRobot* combines optical force transducer technology with high precision 3D actuation (e.g. voice coil, 1 µm encoder resolution; stepper motors, 4 µm feed motion), and customized control software, enabling modular experimentation packages and automated data pre-analysis. In small bundles and single muscle fibres, we demonstrate automated recordings of (i) caffeine-induced-, (ii) electrical field stimulation (EFS)-induced force, (iii) pCa-force, (iv) *slack-tests* and (v) passive length-tension curves. The system easily reproduces results from manual systems (two times larger stiffness in slow over fast muscle) and provides novel insights into unloaded shortening velocities (declining with increasing slack lengths). The *MyoRobot* enables automated complex biomechanics assessment in muscle research. Applications also extend to material sciences, exemplarily shown here for spider silk and collagen biopolymers.

Key words: skeletal muscle, biopolymers, biosensor, biomechatronics, Ca^{2+} sensitivity, elasticity

1. Introduction

Proper function of biomechanically complex skeletal muscle is a crucial prerequisite for quality of life and motility. Activation of muscle motor protein biopolymers, i.e. actin and myosin filaments, is the endpoint of a cascade transforming electrical to chemical and mechanical signals at molecular interfaces that contain, e.g., voltage- or Ca^{2+} ion biosensors (Berchtold et al. 2000). Electrical membrane depolarization and induction of action potentials is followed by a fast signal spread along the muscle fibre membrane. The electrical stimulus is conducted deep into the muscle cell via invaginating t-tubular membrane systems to ensure synchronized activation of contractile biopolymers. Within the tubular membrane, voltage biosensors (dihydropyridine receptors, DHPR) are directly juxtaposed to intracellular Ca^{2+} release channels (ryanodine receptors type 1, RyR1) on the membrane of the sarcoplasmic reticulum (SR), a large internal Ca^{2+} store. The physical interaction between voltage biosensor DHPR and release channel RyR1 is called excitation-contraction (ec) coupling. It translates electrical voltage sensor activation into a transient chemical Ca^{2+} signal through SR Ca^{2+} release. Myoplasmic rise in Ca^{2+} ions during these Ca^{2+} transients activates the contractile biopolymers through troponin-C, acting as a molecular Ca^{2+} ion biosensor to initiate mechanical cross-bridge cycling and filament sliding (Berchtold et al. 2000). This Ca^{2+} biosensor represents a second interface translating chemical to mechanical signaling in muscle. It also represents one of the most sensitive sensors for Ca^{2+} ions with a dynamic range of ~100 nM to ~50 µM (Sun et al. 2006), even outperforming ion selective Ca^{2+} electrodes (Alizadeh et al., 2016). On the single protein level, isolated actin-myosin polymers can be reliably activated in *in vitro* systems and have been employed as Ca^{2+} sensitive molecular shuttles in bio-nanotechnology applications (Sundberg et al., 2006; Mansson et al., 2008).

Muscle function is assessed by its active contractile performance **(Fig. 1A)**. Depending on external load, shortening velocity, force and power vary substantially (Fitts et al., 1998; Josephson & Edman, 1998). Apart from active biomechanical parameters, also passive visco-elastic parameters crucially impact on overall biomechanics **(Fig. 1A)**. Passive strain elements are represented by many linker proteins, both intracellular filaments and extracellular matrix proteins that connect adjacent cells as well as the cytoskeleton from within (Horowits et al. 1986) **(Fig. 1)**. In particular for muscle diseases which almost exclusively present with the very same symptom - muscle weakness -, it is important to unravel the origin of impaired power performance which can either lie within the active contractile apparatus or within cytoskeletal/membrane elements defining passive muscle compliance and stiffness.

Obtaining active/passive biomechanics parameters across different organ levels, in particular from whole muscle, multicellular muscle fibre preparations or single muscle fibres **(Fig. 1B)** is also invaluable to understand disease mechanisms of muscle weakness (Head, 2010; Friedrich et al., 2014), to validate biomechanics in engineered muscle (Moon et al., 2008), etc. For example, extracellular scar tissue is

expected to stiffen the muscle as a whole, but not single muscle fibres after dissection from the organ.

The level of organ scale (whole organ, multicellular preparations and single cells) also impacts on the experimental handling and complexity of techniques required. For example, whole muscle is easily activated by electrical field stimulation (EFS) for twitch and high-frequency tetanic force responses. However, to elucidate intracellular mechanisms with sub-organ resolution, smaller scales at the fibre bundle or single fibre level are often required. This comparative approach allows to dissect contributions from extracellular matrix, ECM (in particular, isolated single fibres no longer connect to ECM), or fibre type variations to recordings (for instance, multicellular preparations contain several cells with diverse myosin heavy chain isoforms, MyHC, while single fibre experiments involving subsequent single fibre biochemistry allow a defined correlation of biomechanics data to a single MyHC isoform in pure fibres). Mechanical skinning of single fibres requires manual cell membrane removal, leaving the resealing t-tubular system functional for EFS with full diffusional myoplasmic access (Posterino et al., 2000). Due to the difficult dissection and custom-made equipment, this technique is currently utilized by only few groups worldwide.

Biomechatronics systems basically exploit measuring isometric muscle force by applying Hooke's law to the deflection of a pin of known stiffness. To this sensor pin one end of the muscle preparation as a linear bioactuator is clamped, while the other side is clamped to a pin of virtually infinite stiffness relative to the stiffness of the force transducer sensor pin **(Fig. 1C)**. The fact that different organ scales and experimentation protocols may be required to completely assess muscle biomechanics in life science research and medical diagnostics represents a huge challenge to biomechatronics technologies available, in particular limiting the automation of most research dedicated to muscle biomechanics. Current commercial muscle biomechatronics systems are tuned for either whole muscle (Hakim et al., 2013), small bundle or single fibre levels (Lynch et al., 2000), either intact or skinned preparations, or for either electrical or chemical manipulation. Besides assessment of active force, passive elasticity requires protocols where translation speed must be either very slow, with high precision and feedback control (~µm range). Slow translation speeds in the range of up to several µm/s ensure that elastic restoration forces and viscous flowing are in equilibrium to yield steady-state elasticity. In contrast, very fast actuation speeds in the range of up to tens of cm/s yield the kinetics for viscous flowing and thus, visco-elasticity, when pulling on muscle fibres, or allow to assess unloaded speed of shortening in so-called *'slack-tests'* (Julian et al., 1986) when pushing on muscle fibres.

Since such experiments on either muscle organ level still require focused involvement of the experimenter with many available systems (in particular monitoring exposure times with stop-watches, manually exchanging between wells in various orders, thus introducing substantial human error) which may not be adjacent, and data processing is often not standardized but manually performed, we sought to

engineer a novel automated biomechatronics system that allows to assess both active and passive biomechanics properties of muscle preparations with programmable interface to perform recordings of (i) chemical SR Ca^{2+} release-induced force transients, (ii) EFS-induced force to activate tubular voltage DHPR biosensors and asses force-frequency curves, (iii) pCa-force curve to assess myofibrillar Ca^{2+} biosensor characteristics, (iv) *slack-tests* to assess unloaded speed of shortening, (v) passive steady-state elasticity resting length-tension curves and (vi) visco-elastic behavior **(Fig. 1B,C)**. The objective was to cover as many experimental protocols as possible with a versatile programmable execution platform, being able to record from several organ scales (single fibres to whole muscle), and to objectively execute biomechanics runs with no manual intervention during recordings. In addition, manual systems (such as the one shown in **Fig. 1D** from previous biological studies of ours) are prone to artifacts by vibration and coarse manual operation **(Fig. 1E)**. The advantage of our *MyoRobot* system over conventional systems is that it covers multiple organ scales (whole muscle, multicellular fibre bundles, single fibres) by exchanging the transducer sensor, and exploits highly accurate voice coil actuators for positioning/speed control. The system is also versatile in its applicability to material testing of linear (bio)polymers to assess compliance/stiffness, as exemplarily demonstrated here for naturally harvested spider silk and microfluidics-spun collagen fibres.

2. Methods

2.1. MyoRobot system

Hardware components. The *MyoRobot* system as of our current design is shown in **Fig. 2**. It combines high precision actuators and sensors for high resolution biomechanics recordings in muscle tissue. The main sensor is a piezo-optical force transducer (SI-KG-7B, Scientific Instruments, Heidelberg, Germany) with a pin embedded in a housing containing an illumination LED (light emitting diode). It casts a shadow that is focused onto a linear photodiode array, transducing the needle position to a photodiode. Its voltage is fed into a bridge-amplifier. The characteristics of the sensor needle are: mechanical compliance ~1.5 µm/mN, force detection range 0-10 mN, force noise level 0-1 µN, force resolution 1 µN. Output voltage was calibrated to force using defined weights in the dynamic range of the transducer and was measured as ~1.115 mN/V. Settling oscillatory and frequency transfer functions of the transducer pin were assessed using an abrupt change in load and an oscillation transfer test vibrometer and oscillator (TV 51110, Tira GmbH, Germany), respectively. Dominant settling frequency was ~423 Hz. Sinusoidal frequency transfer was linear up to 600 Hz. Further up to ~850 Hz, the electronics filter limited resonance magnification to ~10 %.

Actuation of x- and y-axis to move experimental wells was implemented with stepper motors (QSH4218-35-26, -40-033, Trinamic Motion Control, Hamburg, Germany) and custom-made translation sledges to drive the multi-well rack (x-axis) and the force sensor/voice coil actuator (y-axis). The intention of the multi-well rack is to provide a linear array of baths containing chemical solutions to induce defined activation or relaxation states of the muscle preparation. Rather than manually placing the muscle preparation in different dishes, the system only requires the position of the following linear well in an x-position array while z-position and thus, immersion depth of the sample is kept constant for each incubation. Force sensor and voice coil (VC) element were both mounted on a drilled aluminum block aligned in the same plane for simultaneous lifting-lowering to exchange wells underneath. The VC was a cylindrical linear actuator element (CAL 12-010-51, SMAC Inc., Maccon GmbH, Munich, Germany) with a 1 µm positioning resolution and a LabView-implementable controller (LAC-10, Maccon) that operates based on magnetic Lorentz-force. During force recordings of the linearly interposed muscle samples as bio-actuator, the VC is driven in positioning feedback control, where the actuator feed current is regulated according to the VC position. This allows very accurate and stable positioning and a constant force balance of the VC system. The precise absolute position is implemented from a calibrated distance table that is converted to a VC feed current. Moreover, the movement can be implemented with defined velocities and accelerations (www.smac-mca.com). VC positioning and velocities were measured and validated using a custom-built triangulation setup consisting of a laser light source and a CCD camera detecting stray light during movement of the VC. Among biomechanics assessments involving VC control, resting length-tension curves involved linearly pulling very slowly on the muscle preparation with a constant velocity of 0.43 µm/s (equivalent to ~2.2 x 10^{-4} L_0/s, covering a 40 % L_0 stretch within ~30 min), while so-called 'slack-tests' (see 2.3. (iv)) involved a very fast VC movement towards the transducer pin at ~250 mm/s. For a typical L_0 of the fibre segment set to ~1.9 mm, 10 % L_0 slacks were imposed within 0.8 ms and larger slacks of 1,000 µm (50 % L_0) within 4 ms. Electric field stimulation (EFS) was performed via a square pulse stimulator (Stim, Scientific Instr., Heidelberg) applying rectangular pulses of any duration from 0.05 ms to 1 s (15 - 20 V, electrode spacing ~0.4 cm) to two platinum wires mounted into a custom-made Perspex frame holder clipped into one of the wells of choice of the multi-well rack. Attenuated versions of the voltage pulse were also fed into the A/D-D/A converter to be recorded by the *MyoRobot* software to align pulse and force responses. A frequency modulator allowed application of the pulse from 0.25 Hz to 150 Hz. Duration of repetitive pulse trains was about 4 s for frequencies up to 1 Hz and then reduced to 1 s for higher frequencies.

System electronics and software. The force transducer data were digitized via an A/D-D/A converter (NI USB-6008, National Instruments, Munich, Germany) connected to the USB hub of a laptop running LabView (version 2012, National Instruments). The resolution of the digitizer was 12-bit and sampling rate was 10 kHz.

A software GUI was written where the continuously recorded sensor data were plotted in a time lapse representation for visual control of recording quality while data were written to hard disk. The actuation sequence of the stepper motors and VC were translated from a table containing well number # and dwell times $t_{\#.}$ In between wells, the y-motor performed a mirrored positioning drive of lifting the transducer/VC and lowering after accomplished well exchange which was performed by the x-axis stepper motor. VC commands were separately set up in a sub-window providing more advanced options for operation. These options allowed to set up the delay time (time before VC movement in a well), the change in resting length given in percent of L_0, or the time the VC maintains its new position.

2.2. Muscle and biopolymer preparations, chemical solutions

To validate the *MyoRobot* system for active and passive biomechanical properties, mouse (*mus musculus*) and rat (*rattus norvegicus*) *M. extensor digitorum longus* (edl) or *soleus* muscle fibre bundles or single fibres were used. In addition, microfluidics-spun collagen and naturally harvested spider dragline silk were used as passive biopolymer materials. Details are given in the supplemental Methods as well as composition of chemical solutions used. RS: release solution. HR: high relaxing solution. LR. Low relaxing solution.

2.3. Chemical and electrical stimulation protocols

Protocols were implemented in a well-number (#) – exposure time ($t_{\#}$)-matrix to sequentially assess active and passive biomechanical properties. Initially, muscle fibre bundles were chemically skinned (saponin 0.01 % w/v) and the SR completely emptied from endogenous releasable Ca^{2+} ions by immersion in RS for 60 s, then 60 s in HR to buffer all excess Ca^{2+}, then back to idle (LR well).

(i) *Caffeine-induced force transients* (bundles and single fibres)*:* with the SR emptied and after defined SR reload, caffeine-induced transient followed by maximum force assessment involved the sequence: 90 s LS – 1 s HR – 60 s LR – 60 - 90 s RS – 10 s HA - 60 s HR. An example of such an experiment is shown for a manual, conventional system in **Fig. 1D** and for the *MyoRobot* recording as comparison in **Fig. 3B**. The sequence chosen was determined from optimization experiments to tune the loading time in LS to achieve an RS-induced force amplitude of approximate $^2/_3$ of the HA peak.

(ii) *Na^+-depolarization-induced force transients* (mechanically skinned fibres): with the SR emptied and subsequently reloaded under polarizing conditions, the t-system voltage sensor was activated by switching to Na^+-based internal solution. The immersion sequence was: 60 s LS – 1 s HR – 60 s LR – 60 - 90 s NaLR – 60 s HR. To compare this depolarization-induced transient to caffeine-induced force and maximum Ca^{2+}-saturating force, this sequence was followed by the same sequence as in (i). An example trace is shown in **Fig. 4A**.

(iii) *Ca^{2+} sensitivity assessment of the contractile myofibrillar biosensor* (bundles and single fibres): since assessment of the Ca^{2+} biosensor at the chemico-mechanical interface of the troponin C level did not involve any SR Ca^{2+} regulation, the muscle preparation was directly immersed in wells containing highly-EGTA buffered internal solutions with decreasing pCa values flanked by HR and HA. Exposure to each pCa lasted for 20 s before proceeding directly to the next well. An example trace is shown in **Fig. 3C**.

(iv) *Electrical field stimulation, force frequency response* (EFS; single mechanically skinned fibres): after SR reloading, the fibre was placed in a designated well containing the clipped-in EFS stimulator. While bathed in LR solution, field pulses were applied. Frequency was sequentially increased from 0.25 Hz to 25 Hz and stimulation lasted for between 1 s and 4 s.

(v) *Slack test; speed of shortening* (bundles and single fibres): the *slack test* assumes a constant shortening velocity of muscle fibres upon imposing a sudden small slack to the fibre when isometrically activated (Julian et al., 1986; Larsson & Moss, 1993). Muscle preparations were held at resting length L_0, transferred from the LR idle to HA solution and force recorded until a maximum plateau was reached. Then, the VC actuator was moved at maximum speed towards the transducer pin for a given slack length (5 – 55 %L_0) while force declined to zero. Holding the VC at its new position, force was continuously monitored at 2 kHz high sampling rate until force redeveloped through ongoing fibre shortening, re-establishing isometric force production. When the next steady-state force level was reached, the preparation was dipped into HR solution to remove excess Ca^{2+} and then returned to LR idle where the voice coil pin was returned to L_0 under relaxing conditions before the next slack was imposed. **Fig. 5A** illustrates the procedure.

(vi) *Passive axial elasticity, resting length-tension curves*: in order to assess axial fibre/bundle compliance through resting length-tension curves, under LR relaxing conditions, the VC was driven at very slow speed to stretch the preparation while passive restoration force was sampled at 200 Hz. Since muscle elastic biopolymers also possess viscous properties (e.g. titin), the stretch velocity was optimized to values slow enough to be in a steady-state between instantaneous elastic restoration force and viscous relaxation but fast enough to keep recording time at a minimum. The concept of slow stretch 'ramps' is depicted in **Fig. 6**.

2.4. Data analysis and statistics

Details are given in the supplementary Methods.

3. Results

3.1. Quality of MyoRobot force recordings

Fig. 1D shows a conventional manually operated biomechatronics system (Friedrich et al., 2014). **Fig. 1E** is a representative caffeine-induced force transient, followed by maximum Ca^{2+} activated force and Ca^{2+}-depleted relaxation recorded in a fibre bundle on the manual system illustrated in **Fig 1D**. While the signal-to-noise ratio of this type of recording is normally acceptable, the large artifacts caused by manual solution exchanges may reduce the resolution, and in some instances can cause interference with the analysis of force responses. Additionally, in the absence of automated timing control of fibre incubation in calcium loading solutions and solutions containing myogenically active drugs, the manual systems requires an experienced operator using a stop-watch for timing incubation and changing the position of the rack for wells with specified solution content. This can lead to unconscious biases on the part of the operator; for instance if one is expecting a larger response to a drug using a disease model, the operator may be around a second slower in removing a fibre from the Ca^{2+} loading solution, and *vice versa* with the control (Note: it is often not practicable to double blind the operator when using diseased muscle as the phenotype is apparent to the experimenter during dissection and fibre mounting, for example if fibrosis or fat infiltration is present or if single fibres break more easily). Moreover, measurement of isometric force and visco-elastic and mechanical stability of muscle is dependent on its set length; thus, it is critically important to be able to reliably set L_0. The exquisite precision afforded by the voice coil length controller on our automated *MyoRobot* system allows L_0 to be set reproducibly from fiber to fiber (**Fig. 2**). Our automated system also allows highly precise control of muscle length within several µm which is not available on the old manual systems. This enables high resolution measurement of the visco-elastic properties and mechanical stability of the contractile proteins to be reproducibly and routinely performed, among other biomechanical properties **(Fig. 3A)**. Artifacts caused by crossing the water-air interface between wells and thus, introduce no interference with force recordings used in analyzing contraction kinetics **(Fig. 3B)**.

3.2. Automated myofibrillar Ca^{2+} biosensor characterization with the MyoRobot

Troponin C is the muscle biosensor which binds Ca^{2+} and triggers Ca^{2+}-dependent contractile activation, as illustrated in a pCa-force recording (**Fig. 3C**), where each step increase in $[Ca^{2+}]_{free}$ is followed by a corresponding increase in isometric muscle force. Once again, it should be noted that artifacts caused by crossing the water-air interface between wells introduce no interference with steady-state force recordings used to generate the pCa-force curves. Automated analysis by our customized software creates plots of pCa-force relationships (**Fig. 3C**) alongside with Hill-fits.

3.3. Intact ec-coupling via muscle voltage biosensor activation using the MyoRobot

Caffeine **(Figs. 1E, 3B)** directly opens SR release channels on the intracellular Ca^{2+} store (sarcoplasmic reticulum, SR) allowing an efflux of Ca^{2+} into the myoplasm to bind to troponin C triggering contraction. Saponin-skinning of muscle fibres removes the sarcolemma (surface membrane), rendering the fibres electrically unexcitable due to global membrane permeabilization, thus abolishing tubular membrane potential and voltage biosensor responsiveness. However, SR function is preserved and this provides a valuable methodology for probing this SR function **(Fig. 3B)**. In contrast to chemical skinning of the fiber, mechanically removing the sarcolemma seals the t-tubular electrical conduction pathway (**Fig. 4A**) allowing Ca^{2+} release to be triggered directly from the SR by depolarizing, Na^{+}-based solution. This allows the excitation-contraction coupling pathway to be studied **(Fig. 4B)**. The short, transient force response demonstrates responsive ec-coupling. The subsequent force transient (following SR-reloading) was caffeine-induced, triggering complete release of all releasable SR Ca^{2+}. Finally, this was followed by direct stimulation of the contractile proteins by exposing them to a Ca^{2+} saturated intracellular solution in order to measure the maximal isometric force produced by this preparation. This preparation is also an electrical field stimulation (EFS) frequency biosensor that can be used to assess force-frequency curves quantifying the frequency-dependence of Ca^{2+} release correlated to the force produced by the Ca^{2+} release at each stimulation frequency **(Fig. 4B)**. For the single fibre shown (0.25 - 20 Hz), force responses followed stimulation patterns at low frequencies, started to superpose into unfused tetani, and became a more fused tetanus from 10 Hz. The force-frequency curve **(Fig. 4B)** reflects a typical sigmoidal sensor curve, similar to force-frequency curves generated in intact muscle preparations.

3.4. Assessment of shortening speeds using the MyoRobot

While the *slack test* method can assess 'unloaded speed of shortening', it relies on the assumption that there is a constant velocity of shortening during taking up the sudden 'slack' applied to the fibre. Previous studies have only employed small slacks (a few percent of fibre segment length L_0). This is because the fast actuators that are required to outrun shortening of a fast-twitch muscle (several mm/s) have not been available on the "old" manual systems. Our voice coil (VC) actuator allows speeds of ~250 mm/s (equivalent: ~130 L_0/s). This enabled us to extend slack range beyond 50 % of L_0. **Fig. 5B** shows force re-development traces in a small bundle of fast-twitch fibres for given slack lengths $\Delta L(\Delta t)$ between 10 % and 55 % L_0 (inset: full trace for 10 % L_0 recording) in an edl fibre bundle. Slack time Δt to cross the 5 % maximum force threshold increases with ΔL. Our *MyoRobot* software extracts $\Delta L(\Delta t)$-Δt relationships **(Fig. 5C)** and fits bi-exponential curves, defining a fast- and slow-phase. In the fast- and slow-ranges, slope velocity is ~14 mm/s for small slacks and ~1.5 mm/s for large slacks. **Fig. 5D** summarizes data from several small fast-twitch fibre bundles and single fibres. Interestingly, there is an overall higher shortening

velocity for single fibres over fibre bundles, both for the initial unloaded and the subsequent slow phase (P = 0.04).

3.5. MyoRobot automated assessment of axial muscle and biopolymer elasticity

The in-built voice coil actuator allows precise motion at many speeds, including very slow speed (~0.4 µm/s) which was implemented to apply quasi-static passive stretch to muscle **(Fig. 6A)** and biopolymer fibres. Here, we used microfluidics-spun collagen and natural spider silk **(Fig. 6B)** to derive passive axial compliance from resting length-tension curves. In muscle, compliance is initially high (around 10 m/N), as reflected by a rather low restoration force that increases strongly for larger stretches, indicating declining axial compliance (around 2 m/N for 40 % stretch). Linear fits to 10 % L_0 stretch bins, performed both manually and by applying our algorithm (R Studio) to calculate compliance, confirmed the veracity of our automated approach. We used the *MyoRobot* to confirm earlier reports of a decrease in compliance with stretch and an overall two-times larger stiffness (i.e. smaller compliance) in slow-twitch over fast-twitch muscle fibres **(Fig. 6A)**. Moreover, we used the *MyoRobot* to compare force-strain relationships in microfluidics-spun single collagen fibres and naturally harvested *Nephila edulis* spider silk (which is naturally produced as double fibres) **(Fig. 6B)**. Collagen fibres broke at lower strains compared to spider silk fibres. Occasional ruptures of one fibre within the double fibre silk thread were seen as a sudden dip in the force-strain curve **(Fig. 6B)**.

4. Discussion

The role of skeletal muscle not only involves the mechanical endpoints of force and movement, but also biosensor functions at electro-chemical and chemical-mechanical interfaces. Moreover, passive stretch provides differential information on muscle visco-elasticity across organ scales, due to absence/presence of interconnecting matrix when comparing single fibres with multicellular or whole muscle preparations. The generation of genetically modified mouse models mimicking human muscle diseases has led to a renaissance in the study of these conditions with the aim of elucidating their pathophysiology and developing new treatments. Although delicate experimental protocols were developed in the past, currently available commercial biomechatronics systems have limited versatility for the complete investigation of myopathies at functional and structural levels. Biomechanical single fibre studies have become rare due to high levels of training and skills required by the experimenter and limited hardware/software versatility of biomechatronics systems. Early systems involved capacitive force transducers and manual micro-screws for stretching whole muscles (Moss & Halpern, 1977). Other designs included isotonic levers for ‘quick release’ of muscle length involving coil-springs under various loads (Edman & Kiessling, 1971). Using early electromagnetic coils displacement transducers in servo-controlled feedback loops, positioning

achieved ~5 µm accuracy at velocities of ~200 mm/s for sudden length changes (Edman, 1975, 1979), more than ten times the maximum shortening velocity of fast-twitch muscles (Friedrich et al., 2010). Thus, small length changes of ~0.2 mm were performed within ~1 ms rise time (Edman, 1979). The precision provided by current electromagnetic VC technology is also required for very slow and accurate pulling rates on muscle fibres or linear biopolymers. We engineered this technology into a software-controlled environment, using piezo-optical force transducers and 3D mechanical actuation, enabling our *MyoRobot* platform to allow sequential, automated active/passive skeletal muscle biomechanics recordings across organ scales, or for material testing of linear polymers, at very low noise. Automated recording and precise assessment of elasticity parameters is a major advancement over existing biomechatronics systems.

4.1. MyoRobot active muscle biomechanics assessment

Low-noise *MyoRobot* recordings of caffeine-induced force transients and maximum direct Ca^{2+} activation in small bundles (~five single fibres) with amplitude of ~0.6 mN compare well with ~0.1 mN per single fibre using a manual custom-built system (Plant & Lynch, 2002). We also demonstrate control over the releasable SR Ca^{2+} content to ~ 65 % physiological endogenous filling (Lamb et al., 2001). Using a commercial, stepper motor-driven system (Aurora Scientific, model 403A) on permeabilized mouse edl single fibres (cross-sectional area ~2,500 µm²), maximum force was ~0.2 mN (pCa 4.5) and specific force (sF) ~80 kPa (Mendias et al., 2011). Those numbers scale well with maximum forces obtained in our small fibre bundles (~1.0 – 1.4 mN). Although there are studies demonstrating higher maximum tetanic force values (up to 300 kPa, Zhang et al., 2006), there is large variability even within studies (e.g. ~100 kPa, Fig. 1, vs. ~240 kPa, Fig. 2, both single mouse edl fibres, Andrade et al., 1998). Nevertheless, the primary aim here was to demonstrate the appropriateness of our system to automated maximum force detection. Future applications to specific biological models will produce more standardized data to address muscle biomechanics in health and disease.

Characterizing the troponin-C Ca^{2+} biosensor shows typical staircase-patterned force responses when exchanging pCa **(Fig. 3C)** as in manual (Friedrich et al., 2014; Head, 2010) or commercial systems (e.g. Aurora Scientific, model 312C) (Nelson & Fitts, 2014). In particular, our automated actuation to wells of decreasing pCa and force registration produced very robust recordings (negligible baseline drift, complete return to baseline force upon fibre relaxation, **Fig. 3)**. Ca^{2+} sensitivity with half-activation at ~2.5 µM compares well with studies using manual custom-made (Williams et al., 1993) or commercial force recording systems (Scientific Instr., Heidelberg, Germany, Warren III et al., 1996), although there is variability in literature (depending on temperature, pH, ionic strength, sarcomere length, fibre type, etc). Apart from underlying discrepancies of methods to determine or predict the free Ca^{2+} concentrations in Ca^{2+}-buffered solutions (McGuigan et al. 2006), different approaches to fitting of pCa-force curves may account for this (Walker et al. 2010).

Again, our recordings demonstrate the appropriateness of our system. Moreover, subsequent pre-analysis functionality to extract and fit pCa-force curves is a novel implementation in our *MyoRobot* system which was robust in manual vs. automated analysis comparisons.

EFS-induced force response confirms an intact ec-coupling cascade, i.e. tubular voltage biosensor responsiveness and subsequent force superposition. Frequency-force recordings are a relatively easy procedure for whole muscle (reflected by a wealth of studies) where half-maximum tetanic force frequencies typically range from 50 to 80 Hz (Head et al., 2014). Single fibre handling, EFS and force measurements however, are extremely cumbersome, explaining their relative rareness confined to a few labs worldwide. One way to demonstrate intact tubular voltage biosensors is by chemical Na^+-depolarization in mechanically skinned fibres, resulting in force transients of ~5 – 15 s duration and ~50 % maximum force (Lamb et al., 2001; Plant & Lynch, 2002; Posterino et al., 2000; Han et al., 2003). This is reproduced with our *MyoRobot* **(Fig. 4A)**. However, this manoeuver does not provide information about Ca^{2+} and force superposition with EFS frequencies. There are only few studies demonstrating rat edl single fibre force recordings for several EFS frequencies from twitch up to 100 Hz (Verburg et al., 2006; Dutka & Lamb, 2007). With our *MyoRobot*, EFS-assessment on various stimulation frequencies is feasible to extract whole electrical biosensor curves. Our example shown with somewhat reduced amplitudes compared with Verburg et al. (2006) and Dutka & Lamb (2007) may reflect partial t-tubular depolarization. Our primary aim here was to demonstrate the versatility of our technology rather than addressing a specific biological research question on EFS in mechanically skinned fibres. On the contrary, EFS-induced force in single fibres fused at 10 Hz (also seen in Verburg et al., 2006, their Fig. 4), and half-tetanic frequency occurred between 2 Hz and 5 Hz, in contrast to whole muscle (Head et al., 2014). Potentially, inhomogeneous field potentials experienced by fibres at opposing surfaces of a whole muscle set between stimulation electrodes (Taeger et al. 2015) may require higher frequencies and/or voltages to recruit all fibres within the volume.

Applied ‘slack-tests to small fibre bundles and single fibres under unloaded conditions demonstrate the versatile potential of VC implementation in our system. The slack application should be faster than the latent period of cross-bridge cycling (~5 – 8 ms) during early tension development (Colombini et al., 2016). Thus, actuator speed is crucial. Applying early technologies to single intact frog muscle fibres with slack lengths ΔL of 0.3 – 0.8 mm, a linear ΔL-Δt relationship was found, yielding ~4 L_0/s (~24 mm/s, Julian et al., 1986). With relatively long frog muscle fibres (~6 mm), this relates to rather small slacks (5 – 13 % L_0). Applying 0.1 - 0.3 mm slacks to human skinned muscle fibres within 1 – 2 ms (15 °C), linear ΔL-Δt relationships suggested unloaded shortening speeds v_u of 0.3 - 3 L_0/s, depending on fibre type (Larsson & Moss, 1993). With an average L_0 ~1.6 mm in that study, this translates to 6 – 18 % L_0 slacks. Finally, recordings in whole mouse edl muscles at slacks between 5 – 15 % L_0 during EFS yielded v_u values of 3 – 6 L_0/s (20 °C),

translating to ~3 - 9 mm/s for given morphometrical data (Crow & Kushmerick, 1983). Although commercial systems currently implement high performance magnet rotary motor displacements with speeds up to ~850 mm/s (300 µm steps at 0.5 µm precision; e.g. Aurora Scientific 315C,322C), studies on extended slacks are not available. Therefore, we validated our *MyoRobot* system more thoroughly to also apply slacks beyond commonly used ~20 % L_0 constraints. This became possible due to the high actuation speeds of around 250 mm/s of the voice coil actuator engineered into our system. We hypothesized that the ΔL-Δt relationship was in fact non-linear rather than usual linear literature representations, mainly resulting from a very restricted slack range. One would expect 'unloaded shortening' at high v_u for very short slacks that would then turn into an 'internal loading' during ongoing shortening for larger slack lengths. Indeed, this is what our *MyoRobot* results show (**Fig. 5**), i.e. a bi-exponential ΔL-Δt relationship defining a fast shortening phase for small ΔL transitioning into a slow phase for larger ΔL (from ~600 µm or ~30 % L_0). By linear approximation to the fast and slow phase, our v_u values of ~8 mm/s are comparable to results from whole mouse edl muscle (up to 20 % L_0 slack) using the commercial Aurora system model 305B, where v_u was between ~15 L_0/s and 9.5 L_0/s (Gittings et al., 2011). Extrapolation of v_u from ΔL-Δt relationships is extremely sensitive to the ΔL range selected and may even be underestimated here using the 200 - 700 µm bin as compared with including slack lengths down to ~130 µm (Larsson & Moss, 1993). Our results from small bundles and single fibres with the extracellular matrix removed suggest that the presence of ECM puts a marked break both on the unloaded initial and the subsequent, internally loaded phase; more so for the latter one. Thus, we show for the first time that extending the slack range to ΔL > 20 % demonstrates non-linear velocity distribution over slack length which provides a new scientific result obtained with our *MyoRobot*.

4.2. Passive muscle and biopolymer biomechanics assessed with the MyoRobot

Muscle passive biomechanics comprises dynamic viscous, visco-elastic and elastic steady-state stiffness/compliance (Mutungi & Ranatunga, 1996). Dissecting their relative contributions depends on the speed of applied stretches. The viscous parts become apparent at high stretch speeds (>1 – 2 L_0/s, Mutungi & Ranatunga 1996a), while the slower the applied stretch, the more elastic the deformation becomes. Viscosity is mainly set by spring-like filamentous titin (Mutungi & Ranatunga, 1996) containing unfoldable Ig-like domains. Passive elasticity of resting muscle is not related to cross-bridge cycling (Mutungi & Ranatunga, 1996), but superposes stiffness contributions from axial components on the single fibre level (cytoskeleton, membrane, extra-sarcomeric proteins, etc.), while ECM also contributes in multicellular preparations. For whole muscle, extensions are still applicable through manual micro-screws in the mm range and reveal typical organ resting length-tension curves (Rossignol et al., 2008), similar to that of many elastic materials in material sciences. On the single fibre or fibre bundle level however, more precise assessment of elastic behavior requires constant stretch at very slow speeds (in the several

hundredths of L_0 range or <1 µm/s), where viscous relaxation and passive elasticity are in equilibrium, e.g. using fine stepper motors. In contrast, studying viscosity requires very fast extensions, such as performed by piezo-electric transducers. In rat *soleus* and edl small fibre bundles, Mutungi & Ranatunga (1996) used a piezo-ceramic transducer or a permanent ring magnet to build an electromagnetic coil as linear transducer to determine a roughly 5 – 10 times higher elasticity (stiffness) in slow *soleus* over fast edl muscle. There were limitations in their methodology as even their slowest stretches were already at 1 – 3 L_0/s and a steady-state resting length-tension curve was not obtained. Elastic stiffness is defined as the slope of the length-tension curve, thus elastic stiffness or compliance are length-dependent rather than a fixed value. In our setting, compliance (the reciprocal of stiffness) was high at small extensions and dropped exponentially with stretch **(Fig. 6A)**. Our extracted values reproduce a roughly two-fold higher absolute compliance in mouse edl over *soleus* muscle, in agreement with findings in rat bundles (Mutungi & Ranatunga 1996). A higher elastic stiffness of *soleus* muscle would support its anti-gravitational function in order to set less extensibility to a given stretch force. Nevertheless, one cannot directly compare those absolute values to those obtained at other organ scales, as they strongly depend on preparation geometry. For instance, linear fits to recordings of steady-state force-length relationships extracted from fast stretches yielded an absolute elastic stiffness ~3.5 N/mm for edl and ~4.3 N/mm for *soleus* mouse whole muscle (Smith & Barton, 2014). Using average fibre diameters of ~35 µm (edl) and 40 µm (*soleus*) (Diermeier et al., 2017) and five fibres per bundle, absolute axial compliances of ~6 m/N (edl) and 2.5 m/N (*soleus*) at 10 % L_0 stretch translate to a Young modulus of ~66 mN/mm² and ~122 mN/mm², respectively, comparable to values from whole muscles (Smith & Barton, 2014). Elastic modulus literature values for both muscles are rare and may even be conflicting. For instance, another study on whole *soleus* muscle assessing tangent stiffness from stepwise extension tests reported values between 200 and 1,100 N/m for several rheological components in the muscle, translating to compliance values in the range of 0.001 to 0.005 m/N (Anderson et al. 2002), three orders of magnitude smaller as compared to values obtained in our small bundle preparations. With the advantage of automated analysis of resting length-tension curves with high confidence, ongoing research using our *MyoRobot* will contribute to more robust reference values. Finally, applying the system to collagen and natural spider silk fibres reliably reproduced literature values with ease (e.g. estimated elasticity modulus of ~6 GPa for *N. edulis* here using published cross-sections; 4 – 10 GPa, Lintz & Scheibel, 2013). As can be seen from these results, skeletal muscle is roughly 30-80 times more compliant than spider silk or collagen, which have high tensile strength.

5. Conclusions

Our *MyoRobot* combines force sensor technology with high-precision actuation to study active/passive multi-scale muscle biomechanics. Its strongest asset lies in higher accuracy of automated routine procedures with modular test modules,

increasing throughput (e.g. for drug testing) and objective execution. Apart from exemplary applications shown here to validate on pCa-force or passive compliance recordings or to provide novel insights into non-linear speed-of-shortening/slack-length relationships, the system is open to more complex protocols (eccentric contractions, force-velocity curves) and awaits application to a realm of biological questions. Unlike other leading commercial systems the *MyoRobot* is a compact integrated turn-key rig which does not require an expensive inverted research microscope. One limitation is still the lack of simultaneous optical assessment of preparation geometry to directly derive Young elasticity modulus from passive recordings or to convert force to stress values in individual recordings. Current R&D work in our labs is addressing this limitation using optical engineering to include in-built imaging. Our system is not limited to muscle, and has a large number of applications in material sciences, for instance to determine passive properties of biopolymer fibres or performance of artificial muscles.

Acknowledgements

Supported by German Federal Ministry of Economy and Energy (ZIM Initiative ‘Zentrales Innovationsprogramm Mittelstand’, #16KN044038) to OF; German Academic Exchange Service (DAAD) to OF and Australian Group-of-Eight (Go8) to SIH. The authors thank Dr. Grit Pöschel (*conmoto* GbR) for support on sensor and actuator technology. The authors disclose project partnership with the SME *conmoto* GbR through the mentioned ZIM grant.

References

Alizadeh, T., Shamkhali, A.N., Hanifehpour, Y., Joo, S.W., 2016. A Ca2+ selective membrane electrode based on calcium-imprinted polymeric nanoparticles. *New J. Chem.* **40**, 8479.

Anderson, J., Li, Z., Goubel, F., 2002. Models of skeletal muscle to explain the increase in passive stiffness in desmin knockout muscle. *J. Biomech.* **35**, 1315-1324.

Andrade, F.H., Reid, M.B., Allen, D.G., Westerblad, H., 1998. Effect of hydrogen peroxide and dithiothreitol on contractile function of single skeletal muscle fibres from the mouse. *J. Physiol.* **509.2**, 565-575.

Berchtold MW, Brinkmeier H, Müntener M. 2000. Calcium ion in skeletal muscle: its crucial role for muscle function, plasticity and disease. *Phys Rev* **80(3)**, 1215-1265.

Colombini, B., Nocella, M., Bagni, M.A., 2016. Non-crossbridge stiffness in active muscle fibres. *J. Exp. Biol.* **219**, 153-160.

Crow, M.T., Kushmerick, M.J., 1983. Correlated reduction of shortening and the rate of energy utilization in mouse fast-twitch muscle during a continuous tetanus. *J. Gen. Physiol.* **82**, 703-720.

Diermeier, S., Buttgereit, A., Schürmann, S., Winter, L., Xu, H., Murphy, R.M., Clemen, C.S., Schröder, R., Friedrich, O., 2017. Pre-aged remodeling of myofibrillar cytoarchitecture in skeletal muscle expressing R349P mutant desmin. *Neurobiol. Aging,* in press.

Dutka, T.L., Lamb, G.D., 2007. Transverse tubular system depolarization reduces tetanic force in rat skeletal muscle fibers by impairing action potential repriming. *Am. J. Physiol. Cell Physiol.* **292**, C2112-C2121.

Edman, K.A.P., 1975. Mechanical deactivation induced by active shortening in isolated muscle fibres of the frog. *J. Physiol.* **246**, 255-275.

Edman, K.A.P., 1979. The velocity of unloaded shortening and its relation to sarcomere length and isometric force in vertebrate muscle fibres. *J. Physiol.* **291**, 143-159.

Edman, K.A.P., Kiessling, A., 1971. The time course of the active state in relation to sarcomere length and movement studied in single skeletal muscle fibres of the frog. *Acta Physiol. Scand.* **81**, 182-196.

Fitts RH, Bodine SC, Romatowski JG, Widrick JJ., 1998. Velocity, force, power and Ca^{2+} sensitivity of fast and slow monkey skeletal muscle fibers. J Appl Physiol 84, 1776-1787.

Friedrich, O., Hund, E., von Wegner, F., 2010. Enhanced muscle shortening and impaired Ca2+ channel function in an acute septic myopathy model. *J. Neurol.* **257**, 546-555.

Friedrich, O., Yi, B., Edwards, J.N., Reischl, B., Wirth-Hücking, A., Buttgereit, A., Lang, R., Weber, C., Polyak, F., Liu, I., von Wegner, F., Cully, T.R., Lee, A., Most, P., Völkers, M., 2014. IL-1α reversibly inhibits skeletal muscle ryanodine receptor. A novel mechanism for critical illness myopathy? *Am. J. Respir. Cell. Mol. Biol.* **50**, 1096-1106.

Gittings, W., Huang, J., Smith, I.C., Quadrilatero, J., Vandenboom, R., 2011. The effect of skeletal myosin light chain kinase gene ablation on the fatigability of mouse fast muscle. *J. Muscle Res. Cell Motil.* **31**, 337-348.

Hakim, C.H., Wasala, N.B., Duan, D., 2013. Evaluation of muscle function of the extensor digitorum longus muscle ex vivo and tibialis anterior muscle in situ in mice. *J. Vis. Exp.* **72**, e50183.

Han, R., Suizu, T., Grounds, M.D., Bakker, A.J., 2003. Effect of indomethacin on force responses and sarcoplasmic reticulum function in skinned skeletal muscle fibers and cytosolic [Ca^{2+}] in myotubes. *Am. J. Physiol. Cell Physiol.* **285**, C881-C890.

Haynl, C., Hofmann, E., Pawar, K., Förster, S., Scheibel, T., 2016. Microfluidics-produced collagen fibers show extraordinary mechanical properties. *Nano Lett.* **16**, 5917-5922.

Head, S.I., 2010. Branched fibres in old dystrophic mdx muscle are associated with mechanical weakening of the sarcolemma, abnormal Ca2+ transients and a breakdown of Ca2+ homeostasis during fatigue. *Exp. Physiol.* **95(5)**, 641-656.

Head, S.I., Houweling, P.J., Chan, S., Chen, G., Hardeman, E.C., 2014. Properties of regenerated mouse extensor digitorum longus muscle following notexin injury. *Exp. Physiol.* **99**, 664-674.

Horowits R, Kempner ES, Bisher ME, Podolsky RJ. 1986. A physiological role for titin and nebulin in skeletal muscle. *Nature* **323**, 160-164.

Josephson, R.K., Edman, K.A.P., 1998. Changes in the maximum speed of shortening of frog muscle fibres early in a tetanic contraction and during relaxation. *J. Physiol.* **507.2**, 511-525.

Julian, F.J., Rome, D., Stephenson, D.G., 1986. The maximum speed of shortening in living and skinned frog muscle fibres. *J. Physiol.* **370**, 181-199.

Lamb, G.D., Cellini, M.A., Stephenson, D.G., 2001. Different Ca2+ releasing action of caffeine and depolarization in skeletal muscle fibres of the rat. *J. Physiol.* **531.3**, 715-728.

Larsson, L., Moss, R.L., 1993. Maximum velocity of shortening in relation to myosin isoform composition in single fibres from human skeletal muscles. *J. Physiol.* **472**, 595-614.

Lintz, E, Scheibel, T., 2013. Dragline, egg stalk, and byssus: A comparison of outstanding protein fibers and their potential for developing new materials. *Adv. Funct. Mat.* **23**, 4467-4482.

Lynch, G.S., Rafael, J.A., Chamberlain, J.S., Faulkner, J.A., 2000. Contraction-induced injury to single permeabilized muscle fibers from mdx, transgenic mdx, and control mice. *Am. J. Physiol. Cell Physiol.* **279**, C1290-C1294.

Mansson, A., Balaz, M., Albet-Torres, N., Rosengren, K.J., 2008. In vitro assays of molecular motors – impact of motor-surface interactions. *Front. Biosci.* **13**, 5732-5754.

McGuigan, J.A., Kay, J.W.; Elder, H.Y., 2006. Critical review of the methods used to measure the apparent dissociation constant and ligand purity in Ca2+ and Mg2+ buffer solutions. *Prog. Biophys. Mol. Biol.* **92**, 333-370.

Mendias, C.L., Kayupov, E., Bradley, J.R., Brooks, S.V., Claflin, D.R., 2011. Decreased specific force and power production of muscle fibers from myostatin-deficient mice are associated with a suppression of protein degradation. *J. Appl. Physiol.* **111**, 185-191.

Moon du, G., Christ, G., Stitzel, J.D., Atala, A., Yoo, J.J., 2008. Cyclic mechanical preconditioning improves engineered muscle contraction. *Tissue Eng. Part A* **14(4)**, 473-482.

Moss, R.L., Halpern, W., 1977. Elastic and viscous properties of resting frog skeletal muscle. *Biophys. J.* **17**, 203-228.

Mutungi, G., Ranatunga, K.W.,1996. The viscous, viscoelastic and elastic characteristics of resting fast and slow mammalian (rat) muscle fibres. *J. Physiol.* **496.3**, 827-836.

Mutungi, G., Ranatunga, K.W., 1996a. The visco-elasticity of resting intact mammalian (rat) fast muscle fibres. *J. Muscle Res. Cell Motil.* **17**, 357-364.

Nelson, C.R., Fitts, R.H., 2014. Effects of low pH and elevated inorganic phosphate on the pCa-force relationship in single muscle fibers at near-physiological temperatures. *Am. J. Physiol. Cell Physiol.* **306**, C670-C678.

Plant, D.R., Lynch, G.S., 2002. Excitation-contraction coupling and sarcoplasmic reticulum function in mechanically skinned fibres from fast skeletal muscle s of aged mice. *J. Physiol.* **543.1**, 169-176.

Posterino, G.D., Lamb, G.D., Stephenson, D.G., 2000. Twitch and tetanic force responses and longitudinal propagation of action potentials in skinned skeletal muscle fibres of the rat. *J. Physiol.* **527**, 131-137.

Rossignol, B., Gueret, G., Pennec, J.P., Morel, J., Rannou, F., Giroux-Metges, M.A., Talarmin, H., Gioux, M., Arvieux, C.C., 2008. Effects of chronic sepsis on contractile properties of fast twitch muscle in an experimental model of critical illness neuromyopathy in the rat. *Crit. Care Med.* **36**, 1855-1863.

Smith, L.R., Barton, R.R., 2014. Collagen content does not alter the passive mechanical properties of fibrotic skeletal muscle in mdx mice. *Am. J. Physiol. Cell Physiol.* **306**, C889-C898.

Sun, Y.B., Brandmeier, B., Irving, M., 2006. Structural changes in troponin in response to Ca2+ and myosin binding to thin filaments during activation of skeletal muscle. *Proc. Natl. Acad. Sci. USA* **103**, 17771-17776.

Sundberg, M., Bunk, R., Albet-Torres, N., Persson, F., Montelius, L., Nicholls, I.A., Ghatnekar-Nilsson, S., Omling, P., Tagerud, S., Mansson, A., 2006. Actin filament guidance on a chip: toward high-throughput assays and lab-on-a-chip. *Langmuir* **22(17**), 7286-7295.

Taeger, C.D., Friedrich, O., Dragu, A., Weigand, A., Hobe, F., Drechsler, C., Geppert, C.I., Arkudas, A., Münch, F., Buchholz, R., Pollmann, C., Schramm, A., Birkholz, T., Horch R.E., Präbst, K., 2015. Assessing viability of extracorporeal preserved muscle transplants using external field stimulation: a novel tool to improve methods prolonging bridge-to-transplantation time. *Sci. Rep.* **5**, 11956.

Verburg, E., Dutka, T.L., Lamb, G.D., 2006. Long-lasting muscle fatigue: partial disruption of excitation-contraction coupling by elevated cytosolic Ca^{2+} concentration during contractions. *Am. J. Physiol. Cell Physiol.* **290**, C1199-C1208.

Walker, J.S., Li, X., Buttrick, P.M., 2010. Analysing force-pCa curves. *J. Muscle Res. Cell Motil.* **31**, 59-69.

Warren III, G.L., Williams, J.H., Ward, C.W., Matoba, H., Ingalls, C.P., Hermann, K.M., Armstrong, R.B., 1996. Decreased contraction economy in mouse edl muscle injured by eccentric contractions. *J. Appl. Physiol.* **81**, 2555-2564.

Williams, D.A., Head, S.I., Lynch, G.S., Stephenson, D.G., 1993. Contractile properties of skinned muscle fibres from young and adult normal and dystrophic (mdx) mice. *J. Physiol.* **460**, 51-57.

Zhang, S.S.J., Bruton, J.D., Katz, A., Westerblad, H., 2006. Limited oxygen diffusion accelerates fatigue development in mouse skeletal muscle. *J. Physiol.* **572.2**, 551-559.

Figures & Legends

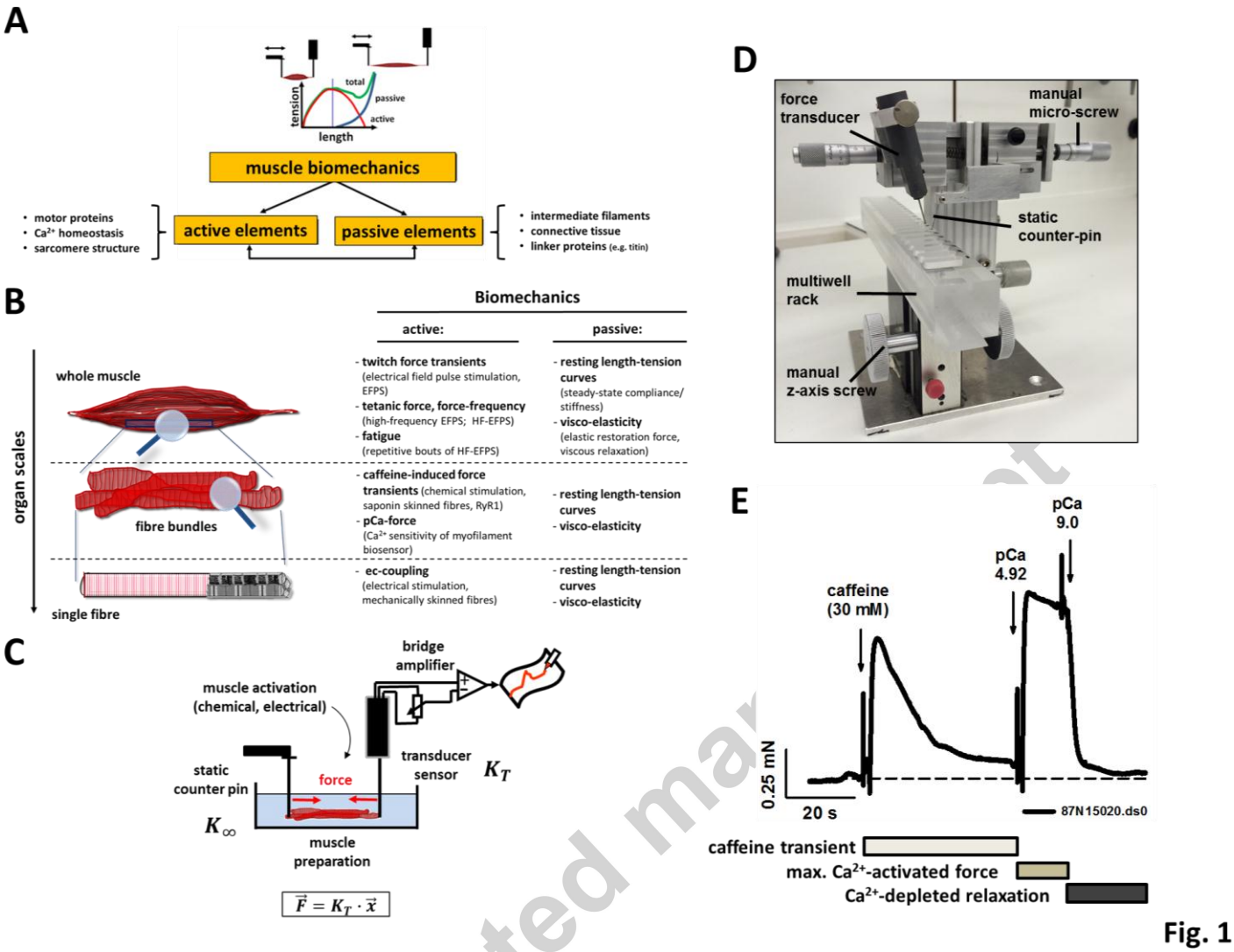

Fig. 1

Figure 1: Muscle biomechanics components, isometric force sensors and conventional manual biomechatronics systems. A, muscle biomechanics is divided into (i) active force-generating elements and (ii) passive elements that convey compliance and stiffness through serially and laterally interlinking proteins. **B,** biomechatronics approaches to asses active and passive biomechanics vary among morphological organ scales and may require different biomechatronics configurations. **C,** isometric force is measured in muscle samples clamped between a sensor element with known stiffness K_T and a static counter pin with infinite stiffness K_∞. Force is converted from transducer pin deflection using Hooke's law. **D,** conventional, manually-operated force transducer system with serial baths for defined chemical muscle activation. Well exchange and muscle sample length changes are manually performed using hand-driven micro-screws that introduce mechanical noise to the recording and/or limit reproducibility due to use of stop watch for bath incubations. **E,** manual recording of caffeine-induced SR Ca^{2+}-release mediated force transients, followed by Ca^{2+} saturating activation of the contractile apparatus and complete relaxation upon Ca^{2+} removal.

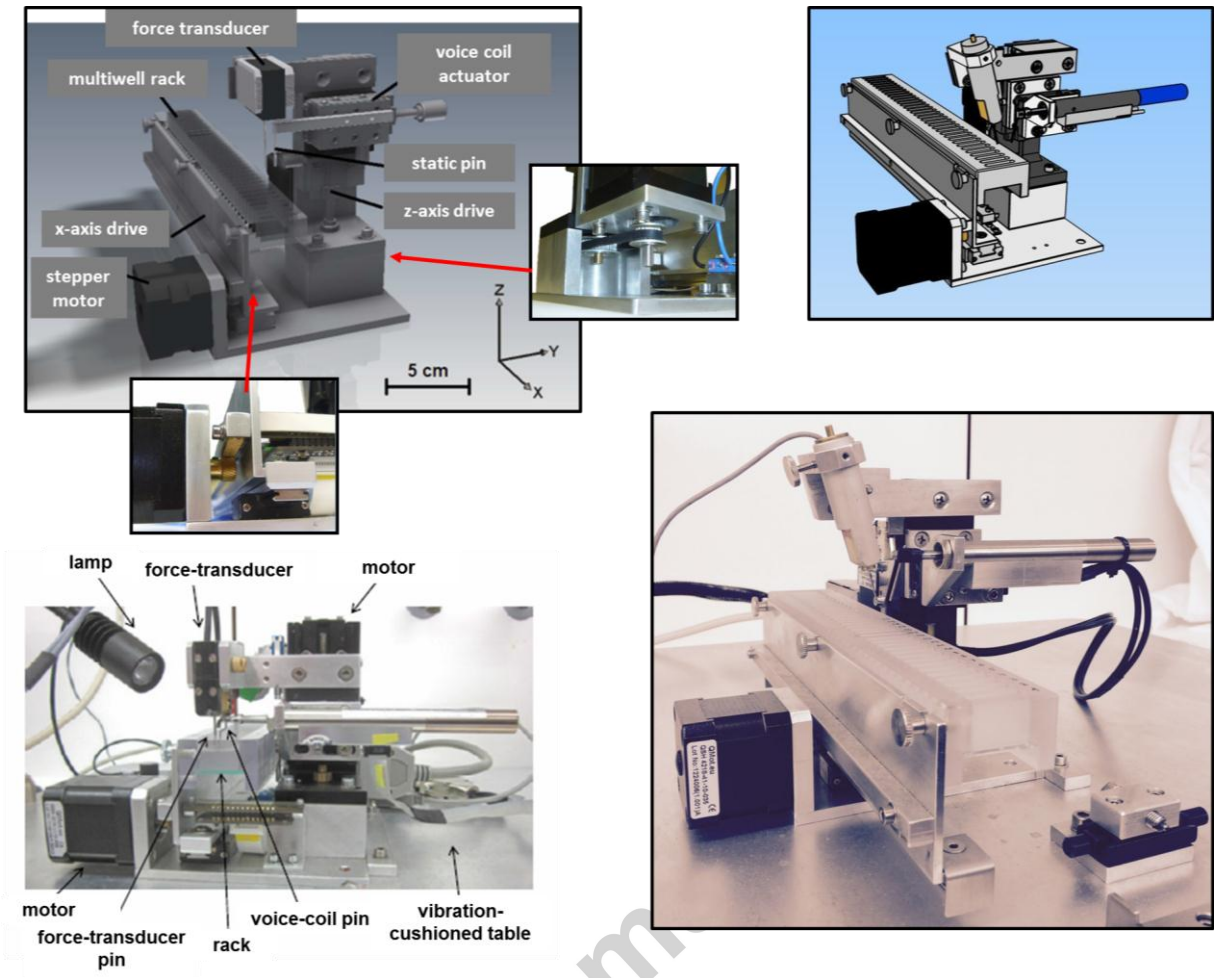

Figure 2: Design and implementation of the *MyoRobot* automated biomechatronics system. Design of linearly arranged bath wells (35 wells milled from Perspex® containing 1 ml of solution each). The multi-well rack is mounted to an aluminum sledge connected to a stepper motor via a sprocket transmitter (inset). The force transducer sensor and the voice coil actuator are both mounted onto a steel block lifted by a stepper motor via a V-belt drive. Thus, changing the well number involves sequentially lifting the transducer/voice coil (y-drive), moving the multi-well rack (x-drive) and lowering the former again. Exposure of the preparation during bath exchange is less than 2 s even between wells spaced 10 wells apart. Voice coil actuation allows accurate and stable µm precision control at very low (~0.4 µm/s) and high speed (250 mm/s). The whole system is controlled via custom-written software.

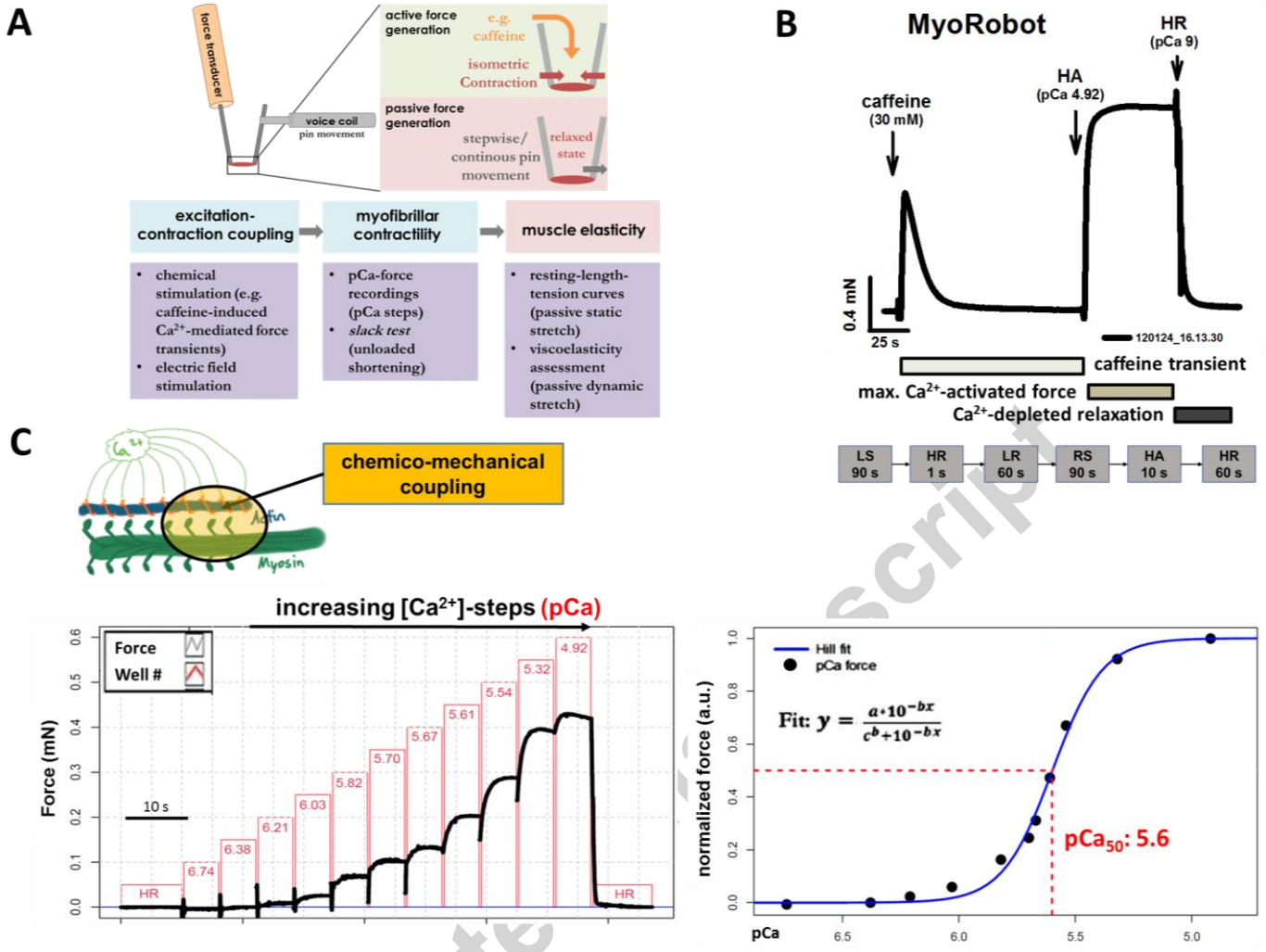

Figure 3: *MyoRobot* assessment of Ca^{2+}-mediated force and contractile biosensor Ca^{2+} sensitivity. A, schematic outline of a typical sequence recording biomechanical parameters, e.g. myofibrillar contractility or biosensor Ca^{2+} sensitivity (active force generation), followed by assessment of muscle elasticity/viscoelasticity (passive force generation). **B,** example of isometric force transients, maximum myofibrillar activation and deactivation in a small mouse edl bundle as in **Fig. 1E**. Note the smooth, artifact-free quality of recordings. Well-time sequence (time spent in each well of indicated solution) shown underneath. **C,** assessment of Ca^{2+} sensitivity at the chemico-mechanical coupling junction by sequent bundle activation in wells with stepwise increasing free [Ca^{2+}]. As expected for a biosensor, the effector variable 'force' exponentially approaches a new steady-state level with altering the control variable '$[Ca^{2+}]_{free}$ (pCa, respectively). The corresponding pCa-force curve represents a typical sensor curve.

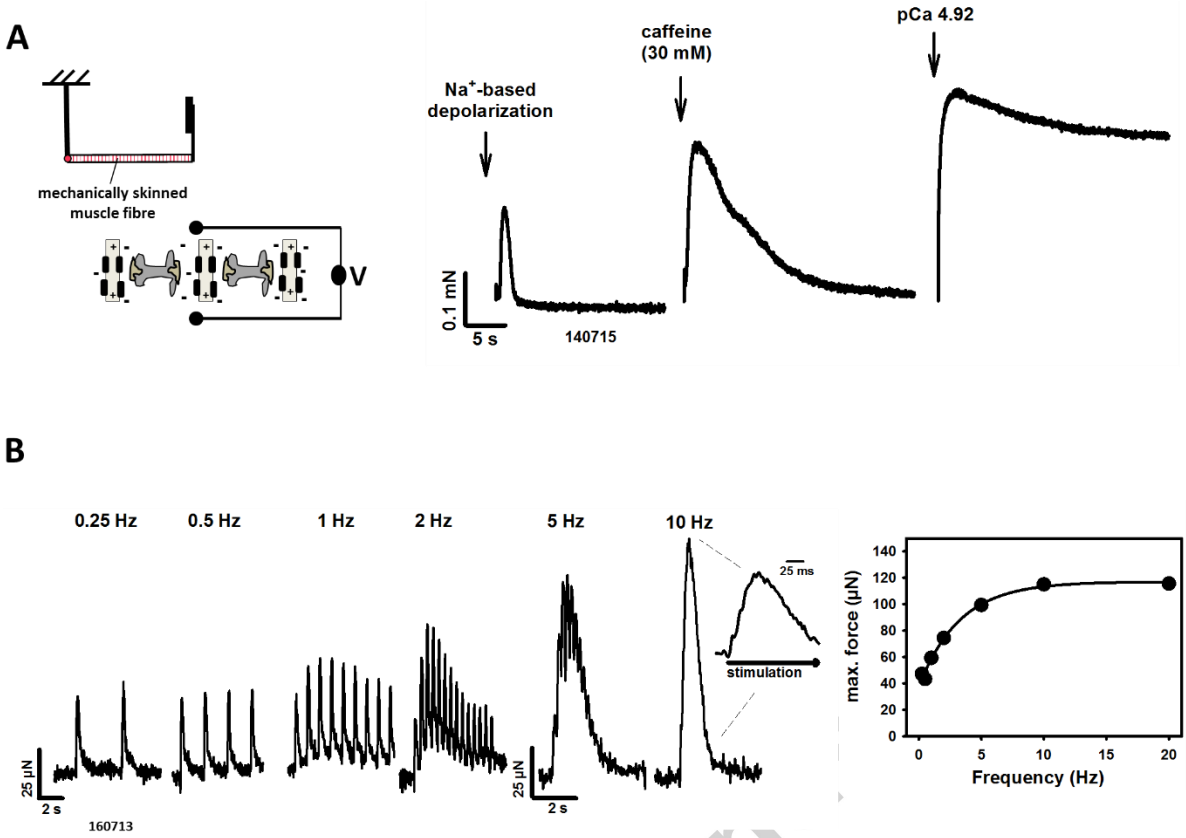

Figure 4: Depolarization-induced force the t-tubular voltage biosensor in single, mechanically skinned rat edl muscle fibres using the *MyoRobot*. A, schematics of a mechanically skinned muscle fibre tied to the force transducer. After peeling back the sarcolemma, t-tubules reseal and repolarize, preserving ec-coupling. This is demonstrated by a chemically induced depolarization: immersing the fibre into a bath containing high Na^+ depolarizes the tubular membrane, releasing Ca^{2+} from the SR via intact ec-coupling. The Na^+-depolarization-induced force transient shows a transient pattern being shorter and smaller in amplitude compared with a subsequent caffeine-induced force transient or sustained direct maximum myofibrillar Ca^{2+} activation. **B,** force-frequency response during EFS of a single fibre demonstrating robust voltage biosensor activation and temporal superposition of twitch force response with stimulation frequency. Numbers beneath the plots refer to experiment identifiers.

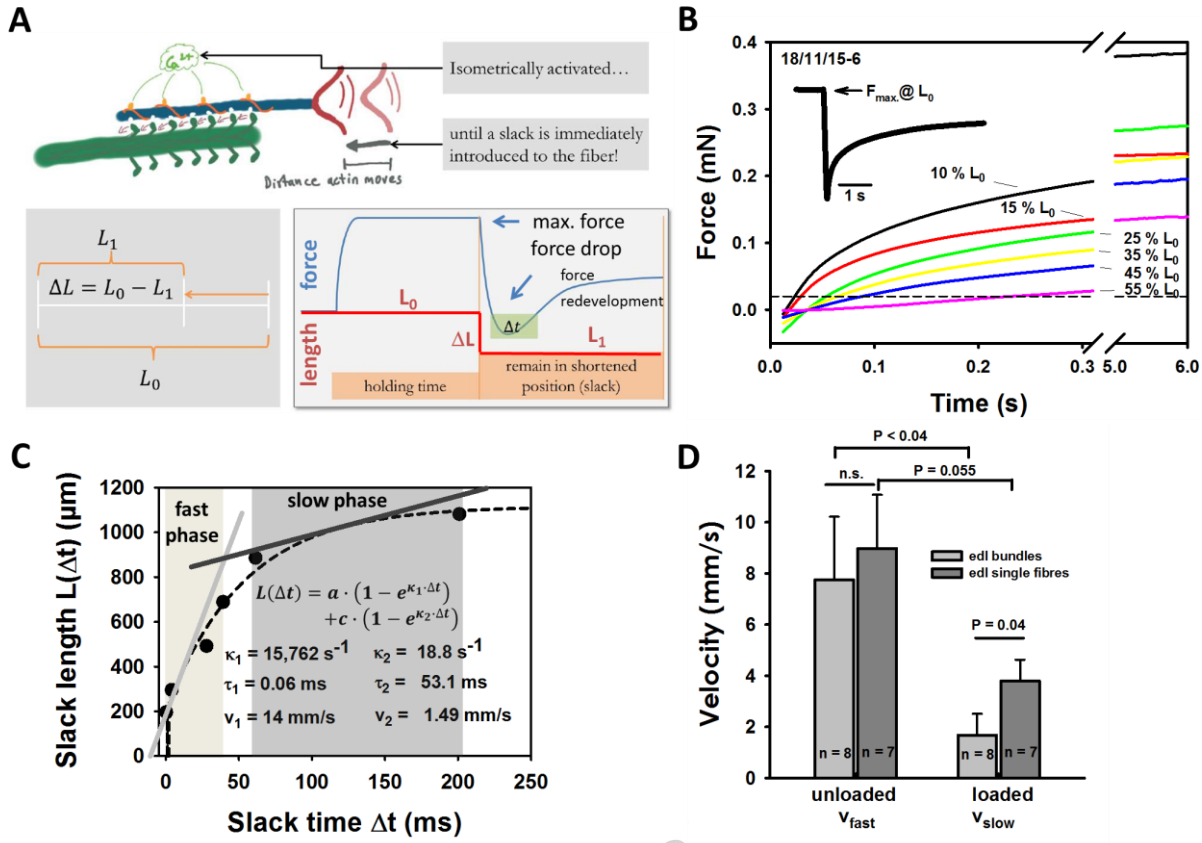

Figure 5: Unloaded speed of shortening assessment using the voice coil actuator to impose fast ‚slacks' on small mouse fibre bundles using the MyoRobot. A, schematic sketch illustrating the ‚slack test' procedure. Following maximum isometric Ca^{2+} activation at resting length L_0, the voice coil actuator is moved for a given ΔL towards the transducer pin at very high speed while force quickly drops from its maximum value to zero at the new length L_1. While the contractile apparatus now contracts without imposed external load, the slack is subsequently taken up until force redevelops, re-establishing isometric contraction at L_1 (see inset trace in (**B**)). The force redevelopment time (‚slack time', Δt) increases with slack length $L(\Delta t)$ (dotted line in (**B**) demarks the 5 % max. force criterion for assessment of Δt). **C,** plotting $L(\Delta t)$- Δt yields a bi-exponential data distribution defining a fast, unloaded shortening phase and a slow, loaded phase. Linear fits to the bi-exponential fit function in each of the two phases yields a fast (v_{fast}) and slow (v_{slow}) velocity. **D,** mean v_{fast} and v_{slow} values from several small fibre bundles versus single fibres demonstrate faster values in single fibres over bundles for both phases.

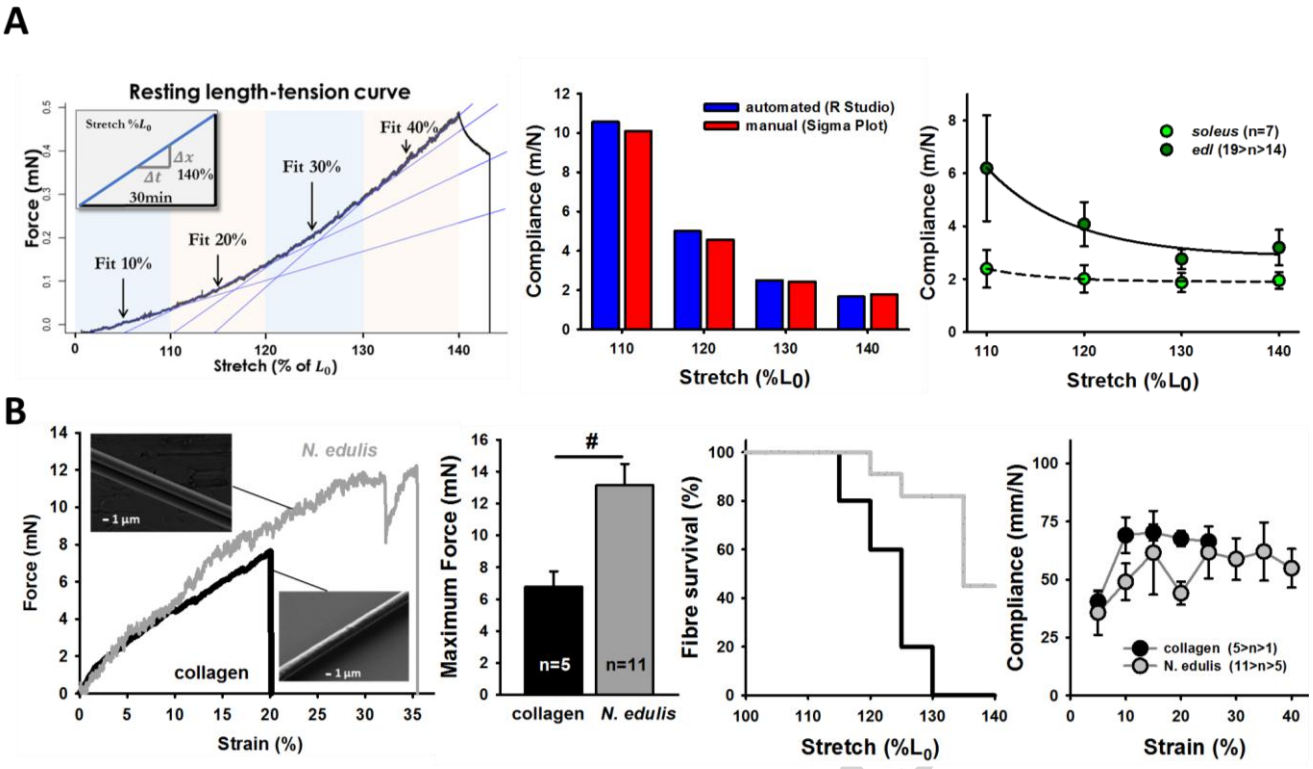

Figure 6: Automated assessment of passive axial muscle and collagen and spider silk fibre compliance using the *MyoRobot* system. A, example resting length-tension recording in a small edl fibre bundle, slowly moving the VC actuator to stretch the preparation and recording increasing restoration force with stretch. Compliance was step-wise determined in 10 % L_0 stretch bins, both via manual calculation and versus automated analysis from the custom-written in-built analysis routine, demonstrating reliability of the *MyoRobot* system. Compliance results obtained from several *soleus* and edl bundles demonstrate an exponentially decreasing axial compliance with stretch and a roughly two-times larger stiffness in *soleus* over edl muscle. **B,** force-strain curves of microfluidics-spun collagen and natural *Nephila edulis* spider silk fibres stretched with the *MyoRobot*. Collagen fibre ruptures at ~25 % strain while for the spider silk double fibre, rupture of the first fibre is seen at ~30 % and total rupture at ~35 %, also reflected by the fibre survival curves. Maximum restoration force before rupture was two-fold higher in spider silk fibres which also survived larger strains compared to collagen fibres. Axial compliance values were comparable between biopolymers, but both being at least 30 times smaller compared to that of muscle preparations.

Highlights Haug et al. (2017)

- An automated, high-precision biomechatronics system, the *MyoRobot*, was engineered
- It assesses single cell, multi-cellular, whole muscle and biopolymer biomechanics
- Sensitivity of the contractile Ca^{2+} ion biosensor is automatically assessed in 2min
- Extracellular matrix puts a brake on unloaded speed of shortening in fibre bundles
- Material parameters of spider silk and collagen fibres were assessed